Analysis of Higher-Order Mode Selection in Rectangular-Shaped VCSELs

A. Gadallah and A. Kroner

We report on the theoretical analysis of a novel type of vertical-cavity surface-emitting laser (VCSEL) that provides selection of a certain higher-order transverse mode. This selection is based on a spatial variation of the threshold gain by adding an antiphase layer with an etched relief structure. The field intensity profile emitted from this laser is calculated numerically as well as with an analytical approach. The main factors that control the selected mode such as the threshold gain, the confinement factor, and the phase parameter are calculated as a function of the active aperture, aiming to achieve single higher-order transverse mode emission. For a given aspect ratio of a rectangular oxide aperture, the threshold gain difference between the selected and neighboring modes is maximized via the relief diameter and the size of the aperture.

1. Introduction

VCSELs have attracted considerable interest due to their low divergence and nonastigmatic beam characteristics as well as low-cost manufacturing, testing and packaging. Besides, the ability of single-mode operation in longitudinal and transverse directions is one of the most distinguished advantages of these lasers. Single-mode VCSELs offer different applications ranging from data transmission to optical sensing [1], [2]. While single-longitudinal mode operation is inherent to the short cavity design of VCSELs, the transverse mode behavior depends on the size of the active aperture as well as the layer structure. To select the fundamental mode, the active aperture of the VCSEL has to be small. This deteriorates the performance of the device by increasing both the thermal resistance and the ohmic series resistance. Moreover, the device lifetime is decreased and mass production is made more difficult due to tight aperture tolerances.

In this report, we introduce a theoretical analysis of VCSELs with rectangular-shaped apertures that allow operation on a certain higher-order transverse mode. The larger aperture size of this VCSEL offers low series resistances as well as potentially increased lifetimes. Another interest of operation on a higher-order transverse mode is in multiple optical trapping [3] and potentially in optical data storage [4].

2. Description of the Device and Theoretical Basics

A schematic drawing of a VCSEL with an etched surface relief is shown in Fig. 1. The layer structure consists of 23 C-doped GaAs/AlGaAs p-distributed Bragg reflector (DBR)

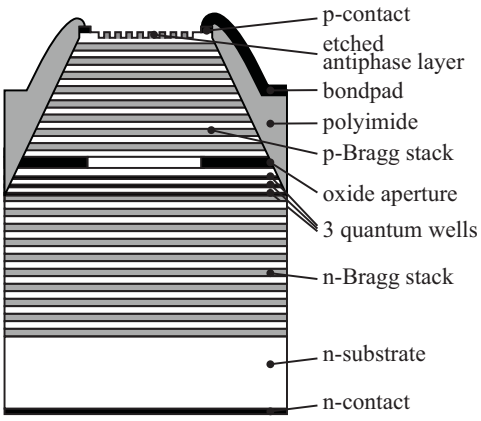

Fig. 1: Schematic representation of a surface-structured VCSEL.

pairs as top mirror (plus the topmost GaAs quarter-wave layer), 38.5 Si-doped n-DBR pairs as the bottom mirror, and three 8 nm thick GaAs quantum wells for laser emission around 850 nm wavelength. The shallow surface relief [1] is utilized to allow operation on a certain higher-order transverse mode. There are two main differences between this specially designed VCSEL and a standard one. Firstly, concerning the layer structure, a quarter-wavelength antiphase layer is added in order to induce a decrease in top mirror reflectivity. This layer is then selectively removed by means of wet-chemical etching. The second point concerns the shape of the mesa and thus of the oxide aperture. It is no longer of circular shape, instead it is rectangular, where one side of the rectangle is much longer than the other. Current confinement is achieved through thermal oxidation of an AlAs layer placed just above the one-wavelength thick inner cavity. Wet etching is used to reach this layer. N- and p- type metalization processes are applied, followed by polyimide passivation. Finally, bondpad metalization is carried out for electrical contacting. In order to investigate the modes that can be excited in such VCSELs, we introduce two different approaches. The first one is based on solving the Helmholtz equation numerically and the second is an analytical solution using the Marcatili approach [5]. For solving the Helmholtz equation numerically, we assume a rectangular core of refractive index n_1, which corresponds to the non-oxidized cross-sectional area of the cavity, is immersed in a cladding layer of refractive index $n_2 < n_1$ [6]. The indices n_1 and n_2 are interpreted as average quantaties in the longitudinal cavity direction. The index difference $\Delta n = n_1 - n_2$ is related to the cavity resonance shift $\Delta\lambda_{\mathrm{ox}}$ as [7]

$$\Delta n = n_1 \Delta\lambda_{\mathrm{ox}}/\lambda \ , \tag{1}$$

where λ is the lasing wavelength. The parameter $\Delta\lambda_{\mathrm{ox}}$ is easily determined from two calculations with the transfer matrix method [7] as the difference in resonance wavelengths in the non-oxidized and oxidized parts of the cavity. With known indices n_1 and n_2, we then numerically solve the Helmholtz equation in the transverse plane while applying the Dirichlet boundary conditions, i.e., the electric field diminishes at the boundary of the calculation window. The result is a usually large number of guided transverse modes. In order to solve the problem analytically and obtain the modes, we refer to Fig. 2, where the active aperture of refractive index n_1 is surrounded by a lower refractive index $n_2 =$

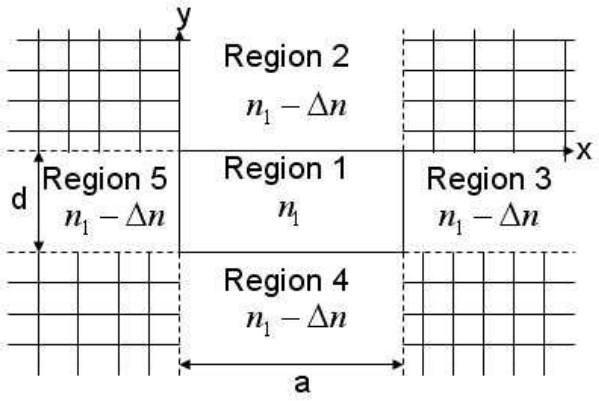

Fig. 2: Approximation of the active aperture of a rectangular-shaped VCSEL with refractive index n_1 surrounded by a lower refractive index medium $n_2 = n_1 - \Delta n$.

$n_1 - \Delta n$, and the fields in the corner regions are neglected according to the Marcatili approximation. The transverse components of the electric or magnetic fields have to satisfy the reduced wave equation

$$\partial^2\psi/\partial x^2 + \partial^2\psi/\partial y^2 + (n_m^2 k^2 - \beta^2)\psi = 0 \ , \tag{2}$$

where ψ is either E_x, E_y, H_x, or H_y and n_m is the refractive index in region m. The propagation constant is $\beta = k n_{\text{eff}}$ with the wavenumber $k = 2\pi/\lambda$ and the effective refractive index in the longitudinal direction n_{eff}. There are two types of modes that such a structure can support, namely E^y_{pq} and E^x_{pq}, where the integers p, q stand for the number of extrema in x- and y-directions, respectively. E^y_{pq} modes are predominantly polarized in y-direction and consist mainly of E_y and H_x. Correspondingly, E^x_{pq} modes are mainly x-polarized with dominant E_x and H_y. The field components E_y and H_x of the modes E^y_{pq} that satisfy (2) in the m-th region in Fig. 2 are given by ([8], p. 49)

$$E_{ym}(x,y) = H_{xm}(x,y) \cdot \begin{cases} (n_1^2 k^2 - k_y^2)/(\omega\epsilon_0 n_1^2 \beta) & \text{for } \ m = 1, \\ (n_2^2 k^2 - k_{y2}^2)/(\omega\epsilon_0 n_2^2 \beta) & \text{for } \ m = 2, \\ (n_2^2 k^2 - k_y^2)/(\omega\epsilon_0 n_2^2 \beta) & \text{for } \ m = 3, \\ (n_2^2 k^2 - k_{y2}^2)/(\omega\epsilon_0 n_2^2 \beta) & \text{for } \ m = 4, \\ (n_2^2 k^2 - k_y^2)/(\omega\epsilon_0 n_2^2 \beta) & \text{for } \ m = 5 \end{cases} \tag{3}$$

and

$$H_{xm}(x,y) = \begin{cases} M_1 \cos(k_x x + \alpha)\cos(k_y y + \varphi) & \text{for } m = 1, \\ M_2 \cos(k_x x + \alpha)\exp(-\mathrm{i} k_{y2} y) & \text{for } m = 2, \\ M_3 \cos(k_y y + \varphi)\exp(-\mathrm{i} k_{x3} x) & \text{for } m = 3, \\ M_4 \cos(k_x x + \alpha)\exp(\mathrm{i} k_{y2} y) & \text{for } m = 4, \\ M_5 \cos(k_y y + \varphi)\exp(\mathrm{i} k_{x3} x + \gamma) & \text{for } m = 5, \end{cases} \tag{4}$$

where the refractive index and the propagation constant in region m are related by

$$k_{xm}^2 + k_{ym}^2 + \beta^2 = n_m^2 k^2 \ . \tag{5}$$

M_m are the field amplitudes, ω is the angular frequency, and ϵ_0 is the permittivity in free space. The angles α, φ locate the field maxima and minima in region 1, and γ equals to

0° or 90°. For matching the fields at the boundaries between region 1 and regions 2 and 4, we have assumed in (3), (4) that

$$k_{x1} = k_{x2} = k_{x4} = k_x \tag{6}$$

and similarly

$$k_{y1} = k_{y3} = k_{y5} = k_y \tag{7}$$

to match the fields between regions 1, 3, and 5. From (3) and (4), the field in region 1 is sinusoidal and decays exponentially in the other regions. Some of the guided transverse

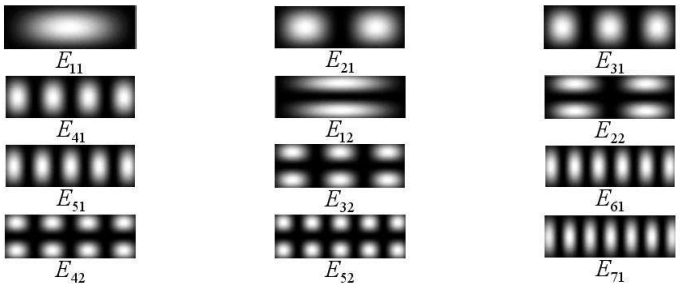

Fig. 3: Intensity profiles of the several guided modes and their designations in a VCSEL with $a = 3d = 30\,\mu m$, $\lambda = 850\,nm$, $n_1 = 3.3$, and $\Delta n = 2 \cdot 10^{-3}$.

modes of such a structure with their mode designations are illustrated in Fig. 3. The corresponding BV diagrams of such a structure generated from the analytical and the numerical solutions for an aspect ratio of 3 are shown in Fig. 4, respectively. The frequency parameter V and the phase parameter B are defined as

$$V = (2\pi/\lambda)d\sqrt{n_1^2 - n_2^2}\ , \tag{8}$$

$$B = (n_{\text{eff}}^2 - n_2^2)/(n_1^2 - n_2^2)\ , \tag{9}$$

where d is the aperture width. From Fig. 4 it is seen that even the fundamental mode E_{11} has a cut-off frequency. Furthermore, the cut-off frequencies of the numerical solutions are smaller than the analytical solutions. As the aspect ratio increases from 3 to 10, the separation between modes on the V-axis decreases, as shown in Fig. 5. In addition, the order of appearance of the modes changes as the aspect ratio changes. The BV diagram for circular aperture VCSELs with the same structure is displayed in Fig. 6. In this case, the parameter d in (8) is identified with the *radius* of the oxide aperture to be consistent with the literature on optical fiber theory. The number of guided modes is low due to the fact that the aspect ratio is equal to one. It is plotted in Fig. 6 (right) as a function of the aperture area. In order to select the oscillation of a certain mode in this VCSEL, for example the mode E_{81}, a shallow one-dimensional relief with 8 circular spots is etched through the entire antiphase layer, such that the centers of the spots coincide with the positions of the extrema of the field profile. Here we assume that the relief does not perturb the field. The selection of the lasing mode of such a structure depends on the confinement factors Γ of the modes and the threshold gains, where

$$\Gamma = P_{\text{p}}/P_{\text{t}} \tag{10}$$

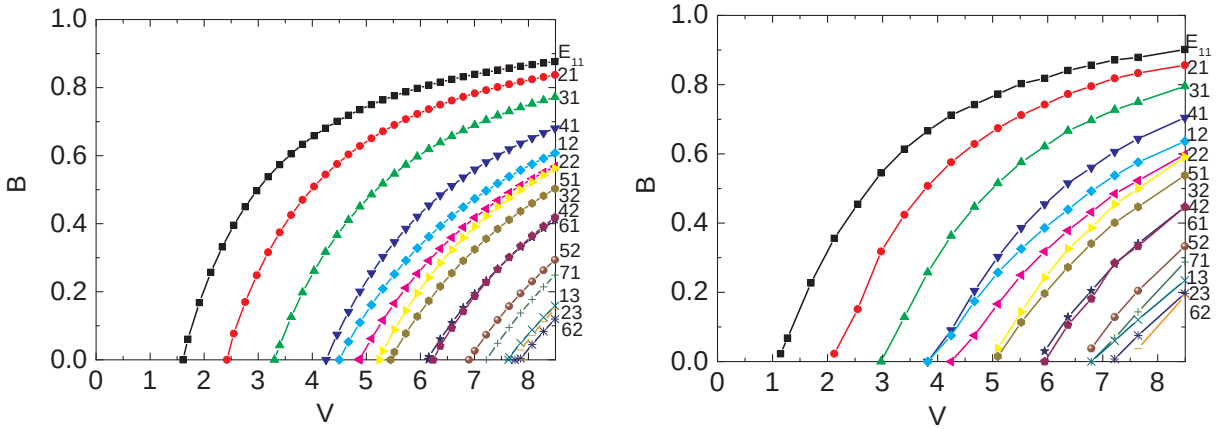

Fig. 4: *BV* diagram of rectangular-shaped VCSELs obtained from analytical solutions (left) and numerical solutions (right). The aspect ratio is 3.

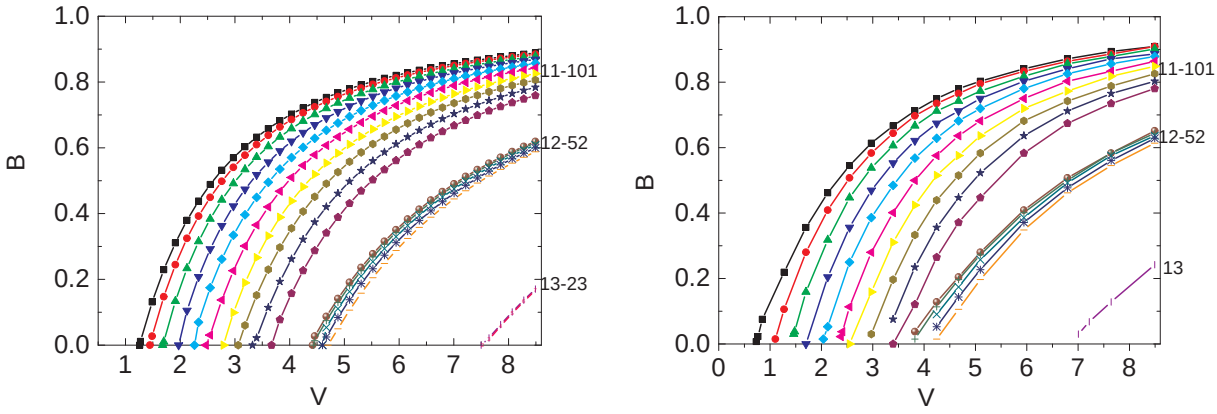

Fig. 5: *BV* diagram equivalent to Fig.4 for an aspect ratio of 10.

with P_p and P_t as the power in area of the etch pattern and the total power of the mode, respectively. The corresponding threshold gain of the mode depends on this confinement factor as well as on the threshold gains inside and outside the spot area, namely g_in and g_out, respectively, where $g_\mathrm{in} < g_\mathrm{out}$. These threshold gains are calculated for the given structure using the transfer matrix method [7]. The threshold gain of the particular mode is then given by

$$g_\mathrm{th} = \Gamma g_\mathrm{in} + (1 - \Gamma) g_\mathrm{out} \ . \tag{11}$$

An important parameter to assess the degree of selection of the desired mode is the difference between its threshold gain and that of the most competitive mode. With the confinement factors of the selected and the competitive mode, Γ_s and Γ_c, respectively, it is written as

$$\Delta g_\mathrm{th} = (\Gamma_\mathrm{s} - \Gamma_\mathrm{c}) \cdot (g_\mathrm{out} - g_\mathrm{in}) \ . \tag{12}$$

For an 8-spot relief, the most competitive mode of the E_{81} is the $E_{12\,1}$ mode. The confinement factors of both modes decrease with increasing aperture width, as shown in Fig. 7 (top left) for aspect ratios of 8 and 10. The corresponding threshold gains for these modes on the other hand increase with increasing aperture width, as seen in Fig. 7 (top right), for $g_\mathrm{in} = 850\,\mathrm{cm}^{-1}$ and $g_\mathrm{out} = 3575\,\mathrm{cm}^{-1}$, structure number 1. However, the threshold gain

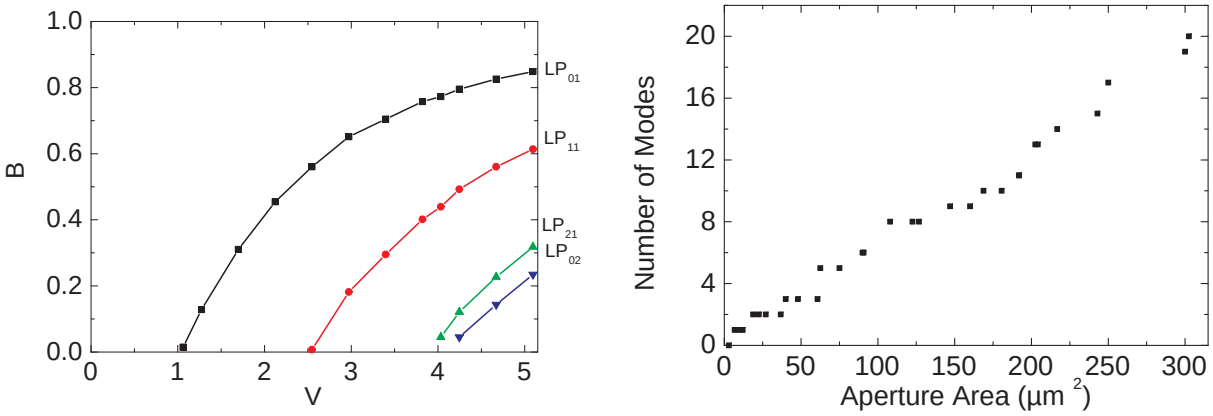

Fig. 6: Numerically calculated BV diagram of circular-shaped VCSELs (left) and the number of modes as a function of the aperture area (right).

difference tends to decrease as the aperture increases. This is shown in Fig. 7 (bottom) for an aspect ratio of 10. In case of a ratio of 8, a slight maximum appears for aperture widths of $d \approx 7\,\mu\text{m}$. From (12) it is understood that mode selection is the better, the higher is the difference in threshold gains inside and outside the etched regions. For this purpose, another structure (number 2) has been utilized with $g_{\text{in}} = 1401\,\text{cm}^{-1}$ and $g_{\text{out}} = 6318\,\text{cm}^{-1}$. The threshold gains of the modes as well as their difference are plotted in Fig. 8 (left). In practice, the higher thresholds of the modes in this structure prevented lasing entirely, and we had to pre-etch the antiphase layer by 16 nm to reduce g_{out} from $6318\,\text{cm}^{-1}$ to $3025\,\text{cm}^{-1}$. The results for this structure (number 3) are shown in Fig. 8 (right). Experimentally, in order to identify the main laser mode, we have performed a spectrally resolved near-field measurement by scanning a lensed fiber tip over the output aperture with high resolution. The obtained pattern is shown in Fig. 9 (left). There are eight intensity maxima in x-direction and one maximum in y-direction, as expected for the E_{81} mode. There is a certain non-uniformity among the peak intensities, however, selection of the lasing pattern. The simulated intensity of this mode is shown in Fig. 9 (right).

3. Conclusions

Using two different approaches, we have investigated the guided modes in oblong-shaped VCSELs. The BV diagrams of such structures are calculated for different aspect ratios. The parameters that control which modes can lase, namely the confinement factors, the threshold gains of the modes, and the gain difference are determined as a function of the aperture width. Three different structures have been utilized to promote operation of a targeted higher-order transverse mode and a first successful experimental demonstration has been made.

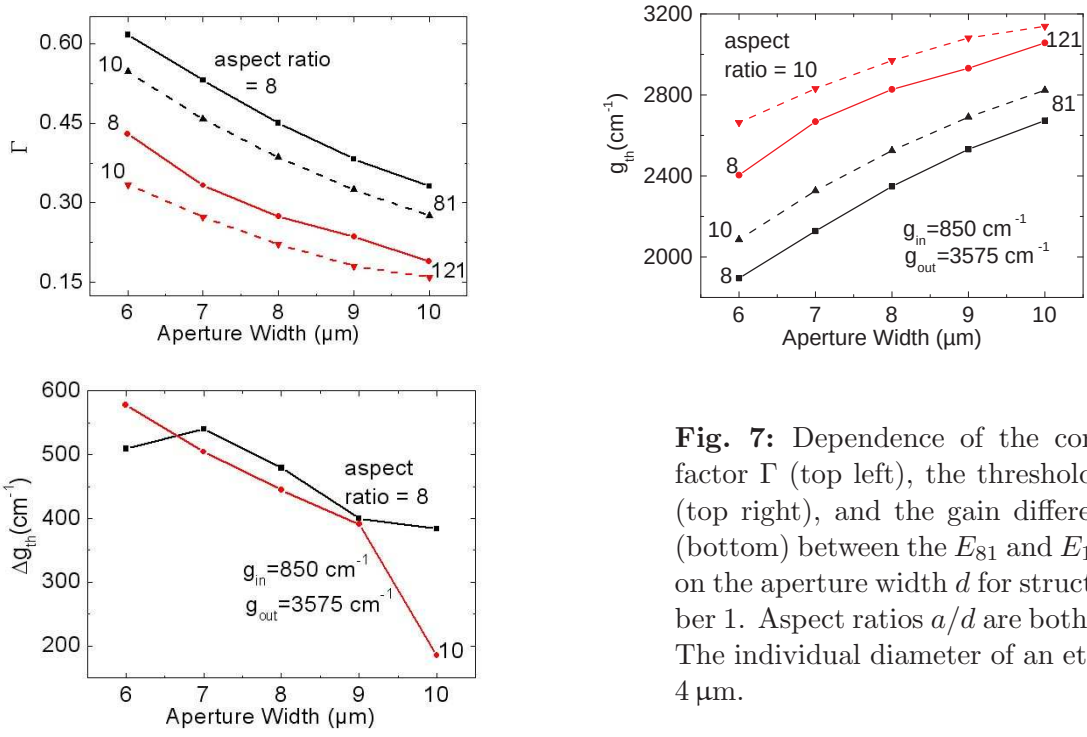

Fig. 7: Dependence of the confinement factor Γ (top left), the threshold gain g_{th} (top right), and the gain difference Δg_{th} (bottom) between the E_{81} and E_{121} modes on the aperture width d for structure number 1. Aspect ratios a/d are both 8 and 10. The individual diameter of an etch spot is 4 μm.

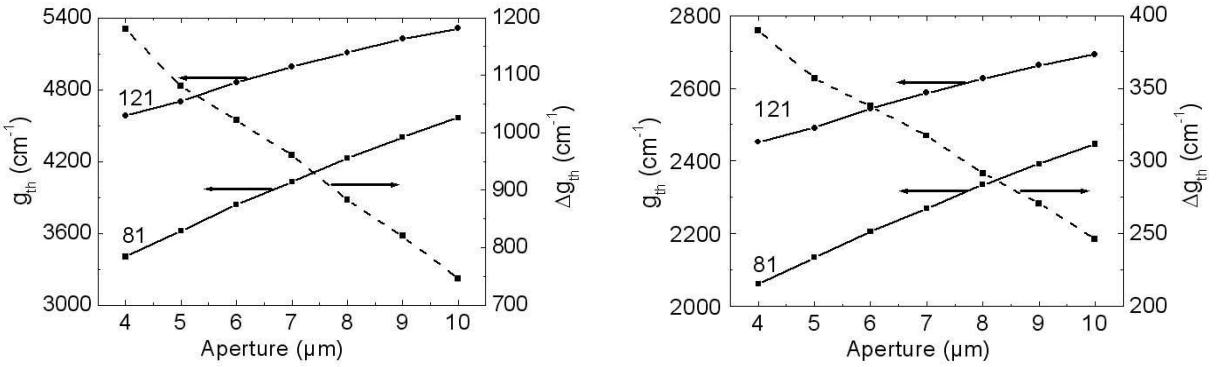

Fig. 8: The threshold gains and their difference in VCSELs with layer structure 2 (left) and structure 3 (right) as a function of the aperture width d for the modes E_{81} and E_{121}. Aperture length and width are related by $a - d = 62$ μm, i. e., the aspect ratio is not constant here.

Acknowledgments

The authors thank U-L-M photonics GmbH for providing the wafer material for some of the studies. Thanks are also due to Ivan Safanov who helped with some useful calculations.

References

[1] H.J. Unold, S.W.Z. Mahmoud, R. Jäger, M. Grabherr, R. Michalzik, and K.J. Ebeling,"Large area single-mode VCSELs and the self-aligned surface relief", *IEEE J. Select. Topics Quantum Electron.*, vol. 7, no. 2, pp. 386–392, 2001.

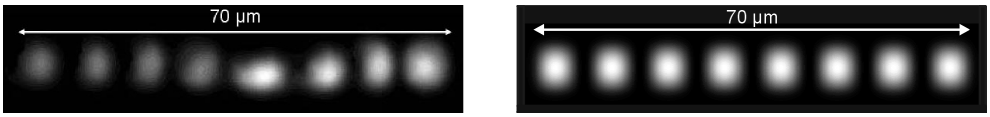

Fig. 9: Measured near-field intensity profile of 8-spot relief VCSELs recorded at 33 mA for structure 1 (left), and the corresponding simulated intensity profile of the selected E_{81} mode (right). The active aperture area is $8 \times 70\,\mu m^2$.

[2] D. Wiedenmann, M. Grabherr, R. Jäger, and R. King, "High volume production of single-mode VCSELs", in *Vertical-Cavity Surface-Emitting Lasers X*, C. Lei, K.D. Choquette (Eds.), Proc. SPIE 6132, pp. 1–12, 2006.

[3] A. Kroner, F. Rinaldi, R. Rösch, and R. Michalzik, "Optical particle manipulation by application-specific densely packed VCSEL arrays", *Electron. Lett.*, vol. 44, 2008, in press.

[4] P.R. Claisse, W. Jiang, P.A. Kiely, B. Gable, and B. Koonse, "Single high order mode VCSEL", *Electron. Lett.*, vol. 34, no. 7, pp. 681–682, 1998.

[5] E.A.J. Marcatili, "Dielectric rectangular waveguide and directional coupler for integrated optics", *Bell Syst. Tech. J.*, vol. 148, pp. 2071–2102, 1969.

[6] R. Michalzik and K.J. Ebeling, "Generalized BV diagrams for higher order transverse modes in planar vertical-cavity laser diodes", *IEEE J. Quantum Electron.*, vol. 31, no. 8, pp. 1371–1379, 1995.

[7] R. Michalzik and K.J. Ebeling, "Operating Principles of VCSELs", Chap. 3 in *Vertical-Cavity Surface-Emitting Laser Devices*, H. Li and K. Iga (Eds.), pp. 53–98. Berlin: Springer-Verlag, 2003.

[8] S.A. Schecanoff, *Electromagnetic Waves*, New York : D. Van Nostrand, p. 94, 1943.